Magnetic ordering effects in the random mixed one-dimensional ferromagnet-antiferromagnet system $RbFeCl_{3-x}Br_x$

1989 J. Phys.: Condens. Matter 1 733

(http://iopscience.iop.org/0953-8984/1/4/008)

J. Phys.: Condens. Matter 1 (1989) 733–754. Printed in the UK

Magnetic ordering effects in the random mixed one-dimensional ferromagnet–antiferromagnet system $RbFeCl_{3-x}Br_x$

A Harrison and D Visser
Oxford University, Inorganic Chemistry Laboratory, South Parks Road, Oxford OX1 3QR, UK

Received 28 April 1988, in final form 3 August 1988

Abstract. Elastic neutron scattering experiments were performed on single crystals of the solid solution $RbFeCl_{3-x}Br_x$ ($x = 0.03$, 0.06, 0.15, 1.0, 2.56, 2.76, 2.85 and 2.94) to study the magnetic ordering behaviour and the magnetic phase diagram of this mixed pseudo-one-dimensional ferromagnetic–antiferromagnetic system. Small amounts of dopant destroy the magnetic long-range order of the pure parent compounds, $RbFeCl_3$ and $RbFeBr_3$. On the $RbFeCl_3$ side of the phase diagram the magnetic correlations appear finite for x as small as 0.03. The periodicities of these correlations are similar to those of the incommensurate and commensurate magnetic phases of pure $RbFeCl_3$. On the $RbFeBr_3$ side of the phase diagram the ordering vector remains at the H point ($\boldsymbol{Q} = (\frac{1}{3}\,\frac{1}{3}\,1)_N$). At an intermediate composition ($x = 1.0$) there are no detectable one-dimensional ferro- or antiferromagnetic correlations down to a temperature of 1.3 K.

1. Introduction

1.1. Engineering insulating spin glasses

Early experimental studies of spin-glass behaviour concentrated on metallic alloys. The combination of quenched spatial disorder and frustration required to impart spin-glass properties to a material (Toulouse 1977, Sherrington 1983) was produced by diluting magnetic atoms in a non-magnetic matrix and exploiting the dependence of the sign of the RKKY exchange constant on the inter-atomic separation. More recently, attention has turned to insulators as bases for spin-glass properties. The short-range nature of the superexchange mechanism allows one to predict the most favourable conditions for spin-glass behaviour using a knowledge of the topology of the important exchange pathways and of the signs of the NN (nearest-neighbour) (and sometimes also the NNN (next-nearest-neighbour)) magnetic exchange constants (Villain 1979).

The following categories emerge:

(i) A solid solution of a NN ferromagnet with a NN antiferromagnet, e.g. $Rb_2Cr_{1-x}Mn_xCl_4$ (Katsumata *et al* 1982, Katsumata 1986, Munninghof *et al* 1984), $K_2Cu_xMn_{1-x}F_4$ (Kimishima *et al* 1986) and $Co_{1-x}Mn_xCl_2.2H_2O$ (Defotis and Mantis 1986).

(ii) Diamagnetically diluted frustrated magnets where the host material has (a) NN

0953-8984/89/040733 + 22 $02.50

antiferromagnetic exchange with an odd number of bonds in some of the loops of exchange pathways, e.g. spinels (Hubsch *et al* 1978) and the pyrochlores $CsMnFeF_6$ (Bevaart *et al* 1983) or $CsNiFeF_6$ (Pappa *et al* 1984); (b) NN and NNN antiferromagnetic exchange, e.g. the pseudo-one-dimensional (1D) antiferromagnet $FeMgBO_4$ (Wiedenmann *et al* 1981, 1983); and (c) NN ferromagnetic and NNN antiferromagnetic exchange, e.g. $Eu_{1-x}Sr_xS$ (Maletta 1982).

In some materials it is believed that spin-glass properties co-exist with long-range or medium-range magnetic order to form a 'semi spin glass'. The predictions of Villain concerning the sort of magnets in which properties may be found have been realised in a number of materials (Brand *et al* 1985, Wong *et al* 1985; but see also Maletta and Felsch 1980, Maletta *et al* 1982, Aeppli *et al* 1982).

Finally, it should be noted that magnetic properties characteristic of a spin glass may be seen in materials that do not have competing magnetic exchange interactions but have random magnetic anisotropy, e.g. $Dy(VO_4)_{1-x}(PO_4)_x$ (Kettler *et al* 1981) and the metallic alloys a-DyFeB (Sellmyer and Nafis 1986).

In this paper we present a single-crystal neutron diffraction study of the mixed ferromagnet–antiferromagnet system $RbFeCl_{3-x}Br_x$. Previous workers (Bontemps *et al* 1982, Visser and Harrison 1982) studied these materials as potential insulating spin glasses, using a combination of magnon side-band and magnetic circular dichroism measurements and powder neutron diffraction. No conclusive evidence was found for spin-glass behaviour. The present study gives a classification of the magnetic structure of $RbFeCl_{3-x}Br_x$ over the full compositional range and at temperatures down to 1.3 K. In order to present clearly the reasons behind the experimental procedure it is necessary to consider the particular magnetic properties of the parent compounds, $RbFeCl_3$ and $RbFeBr_3$.

1.2. Properties of $AFeX_3$ magnets

Both $RbFeCl_3$ and $RbFeBr_3$ adopt the hexagonal perovskite structure in which chains of face-sharing FeX_6^{4-} octahedra lie parallel to the crystal *c* axis. The chains are separated by Rb ions in twinned cuboctahedra (12-fold coordination) which are also stacked in a linear fashion along the *c* axis. The space group is $P6_3/mmc$. At 108 K (Visser 1988b) $RbFeBr_3$ undergoes a phase transition in which two-thirds of the Fe chains (A sites) move by approximately 0.5 Å out of the basal plane, forming a honeycomb lattice (Eibschutz *et al* 1973, Adachi *et al* 1983). The remaining one-third (B sites) lie in a triangular array. The new crystal structure is that of $KNiCl_3$ at room temperature (Visser *et al* 1980) with space group $P6_3cm$ and the cell parameters *a* and *b* enlarged by a factor of $\sqrt{3}$. ABX_3 crystals undergoing phase transitions of this sort have been shown to possess structural disorder in the $P6_3cm$ phase (Visser and Prodan 1980). The structural parameters of $RbFeCl_3$ and $RbFeBr_3$ are given in table 1. In the case of $RbFeBr_3$ at 20 K and 1.5 K the averaged value of the positional parameter, x_{Br}, is given to aid a direct comparison with $RbFeCl_3$.

By virtue of the chain structure the intra-chain exchange constant J_1 is an order of magnitude greater than the inter-chain exchange constant J_2, giving rise to pseudo-one-dimensional magnetic behaviour. In both cases J_2 is antiferromagnetic and induces three-dimensional magnetic long-range order at low temperatures. However, J_1 is very sensitive to the angle α of the intra-chain exchange constant bridge Fe–X–Fe. The bromide has antiferromagnetic J_1 wheras the less covalent chloride, with a larger value

Table 1. Structural parameters for $RbFeCl_3$ and $RbFeBr_3$ as determined by powder neutron diffraction.

Compound	T (K)	a (Å)	c (Å)	x(Cl, Br)	α (deg)	Space group	Source
$RbFeCl_3$	293.0	7.100	6.048	0.1610	75.01	$P6_3/mmc$	[a]
	4.2	6.933	5.954	0.1628	74.09	$P6_3/mmc$	[b]
	1.5	6.933	5.954	0.1628	74.09	$P6_3/mmc$	[a]
$RbFeBr_3$	300.0	7.422	6.304	0.1600	74.28	$P6_3/mmc$	[a]
	150.0	7.380	6.28	0.1643	—	$P6_3/mmc$	[c]
	20.0	12.78	6.28	0.1700[d]	—	$P6_3cm$	[c]
	1.5	12.72	6.263	0.1683[d]	72.45	$P6_3cm$	[a]

[a] Visser and Harrison (1982).
[b] Visser *et al* (1985).
[c] Eibschutz *et al* (1973).
[d] This value is the average of the x parameter for the different halide positions in the $P6_3cm$ space group.

of α, has ferromagnetic J_1. The change in the sign of J_1 has been attributed (Lines and Eibschutz 1975, Eibschutz *et al* 1975) to an increase in the antiferromagnetic 'kinetic' component of superexchange relative to the ferromagnetic 'potential' component.

There are two other important forms of balance between competing magnetic effects in these $AFeX_3$ magnets.

(i) The cubic component of the ligand field acts on the ^5D free-ion term of Fe^{2+} to give a ground singlet $|m_J = 0\rangle$ and an excited doublet $|m_J = \pm 1\rangle$. For an isolated ion the doublet lies at an energy D above the singlet state, but as a magnetic field is applied parallel to the c axis, or through the influence of the inter-ion perturbation provided by superexchange, the excited doublet is mixed into the singlet ground state. In the absence of an applied magnetic field the size of the induced moment depends on the ratio D/J_Q, where J_Q is the magnetic exchange field experienced at a single ion when the configuration of moments has the ordering vector $\boldsymbol{Q}$. For low values of D/J_Q the induced moment may be sufficiently large for magnetic long-range order to occur at low temperatures. Thus, $RbFeBr_3$ and $RbFeCl_3$ show magnetic long-range order at 5.5 and 2.5 K respectively. The caesium salts, with larger unit cells and smaller exchange constants, show no magnetic long-range order down to 80 mK for $CsFeCl_3$ (work reported by D P E Dixon in 1981 and cited by Baines 1983) and 69 mK for $CsFeBr_3$ (Visser 1988a). When a magnetic field is applied along the crystal c axis of $CsFeCl_3$ three-dimensional magnetic long-range order is observed (Knop *et al* 1983) which is similar to that seen in $RbFeCl_3$ (Wada *et al* 1982).

The magnetic exchange parameters for $RbFeCl_3$ and $RbFeBr_3$ are presented in table 2. A survey of the values available in the literature shows them to be very dependent on the type of measurement made and the model used to interpret the data. Thus, we have only used values which have been determined in the most reliable fashion for both compounds. The magnetic susceptibility measurements of Lines and Eibschutz (1975) and of Eibschutz *et al* (1975), interpreted by Lines' correlated effective field (CEF) approximation (Lines 1974), and inelastic neutron scattering measurements, interpreted using the CEF model and Suzuki's dynamical CEF approximation (DCEFA) (Suzuki 1983, Harrison and Visser 1988a), are suitable for this purpose.

Table 2. Magnetic exchange parameters and single-ion anisotropies calculated by previous workers for $RbFeCl_3$ and $RbFeBr_3$. The exchange parameters all refer to an effective spin $S' = 1$ Hamiltonian and all energies are given in meV. The source of the data is given as a superscript letter which tallies with the references below the table. The work of Lines and Eibschutz (1975) and of Eibschutz *et al* (1975) involved the application of the Lines (1974) CEF model to magnetic susceptibility data. The other values were derived from inelastic neutron scattering data using the Suzuki (1983) DCEFA model.

Parameter	$RbFeBr_3$	$RbFeCl_3$
$J_1^{\perp}$	-0.525^a	0.325^c
	-0.394^b	0.405^d
$J_1^{\parallel}$	-0.35^a	0.216^c
	-0.411^b	0.527^d
J_2	-0.008^a	-0.008^c
$J_2^{\perp}$	-0.046^b	-0.034^d
$J_2^{\parallel}$	-0.079^b	-0.045^d
D	1.0–1.1^a	1.0–1.1^c
	1.96^b	1.92^d

[a] Eibschutz *et al* (1975).
[b] Harrison and Visser (1988a).
[c] Lines and Eibschutz (1975).
[d] Suzuki (1983).

(ii) The one-dimensional ferromagnetic intra-chain correlations in $RbFeCl_3$ give rise to an inter-chain magnetic dipole–dipole interaction γ of significant magnitude relative to the intra-chain superexchange constant J_2. The former alone would give rise to a free-energy minimum at the M point of the reciprocal lattice ($\boldsymbol{Q} = (\frac{1}{2}\,0\,0)_N$) and the latter at the K point ($\boldsymbol{Q} = (\frac{1}{3}\,\frac{1}{3}\,0)_N$) (Shiba 1982, Shiba and Suzuki 1983). Competition between these forces leads to the formation of two incommensurate magnetic phases, IC_1 and IC_2, on cooling from the paramagnetic phase to 2.5 and 2.35 K respectively. At 1.95 K a transition to the commensurate 120° configuration occurs (Wada *et al* 1982). The IC phases are characterised in neutron scattering by satellite Bragg peaks centred around the K point, on the KM lines (IC_1 *and* IC_2 phases) and on the KΓ lines (IC_2 phase only). Similar phases have been observed in $CsFeCl_3$ when a magnetic field is applied along the crystal c axis (Knop *et al* 1983) and in $TlFeCl_3$ below 2.02 K (Visser and Knop 1988).

1.3. Structural and magnetic properties of $RbFeCl_{3-x}Br_x$

The search for spin-glass behaviour in the mixed ferromagnet–antiferromagnet $RbFeCl_{3-x}Br_x$ followed the theoretical work of Medvedev and Rumyantsev (1978), Chen and Lubensky (1977) and Fishman and Aharony (1979). These theorists proposed two schematic phase diagrams to describe the magnetic structure of alloys formed by mixing a nearest-neighbour ferromagnet with a nearest-neighbour antiferromagnet. At intermediate compositions and low temperatures the formation of either a paramagnetic phase (figure 1(*a*)) or a spin-glass phase (figure 1(*b*)) is envisaged.

Previous x-ray and neutron powder diffraction measurements (Visser and Harrison 1982) showed that the components of $RbFeCl_{3-x}Br_x$ form a single solid solution. The cell parameters of the mixed compounds at room temperature are those of a hexagonal perovskite with space group $P6_3/mmc$. The neutron diffraction data taken at 1.3 K show that compounds of composition $x > 2.0$ undergo a phase transition similar to that of pure $RbFeBr_3$: the unit-cell parameters a and b enlarge by a factor of $\sqrt{3}$, and the space

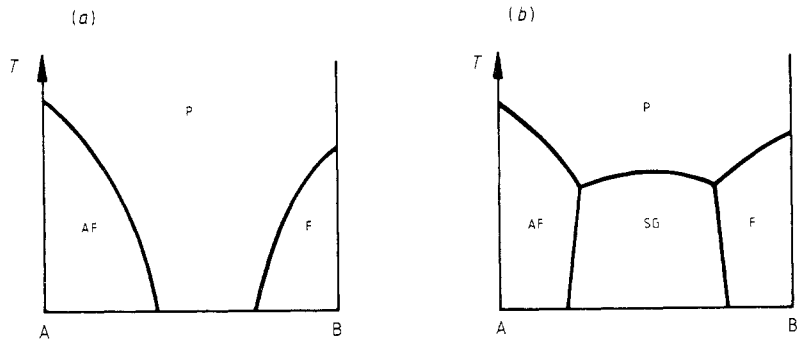

Figure 1. Schematic phase diagram for an alloy of an antiferromagnet (A) with a ferromagnet (B), depicting the possibility of the formation of (*a*) a paramagnetic phase (P) or (*b*) a spin-glass phase (SG) at intermediate compositions. The calculations assume single nearest-neighbour exchange linkages (Fishman and Aharony 1979).

group changes to $P6_3cm$. There was no observable magnetic long-range order down to 1.3 K for compositions with x as low as 0.3 or as high as 2.7.

Bontemps *et al* (1982) performed magneto-optical measurements on $RbFeCl_{3-x}Br_x$ and concluded that for $x = 0.04$, 0.2 and 1.0 the intra-chain exchange constant was not substantially modified relative to that found in the pure chloride. The sample with $x = 2$, however, behaved in a manner which could not be described simply as a mole-fraction-weighted average of the parent compounds' behaviour. This was attributed to extensive magnetic disorder in $RbFeClBr_2$. The position and intensity of the optical absorption bands of $RbFeCl_{3-x}Br_x$ changed gradually with composition between the values measured for the pure compounds. This also indicates that $RbFeCl_{3-x}Br_x$ behaves as a solid solution.

The compounds $RbFeCl_3$ and $RbFeBr_3$ differ in two respects from the end-members of the phase diagrams drawn up by Fishman and Aharony (1979). First, the induced-moment nature of the compounds introduces another possible phase to the diagram—namely a singlet ground-state phase. Secondly, the nature of the superexchange between two Fe^{2+} ions connected by a mixture of halide ions is unknown at the microscopic level. The average macroscopic exchange is known and is described below. It is likely that for a wide range of compositions there will be a distribution of intra-chain exchange constants ranging from positive to negative values. Some spin-glass character is expected so long as the impurities do not disrupt the exchange field to such an extent that the induced moments are destroyed. Consequently, spin-glass behaviour is more likely on the $RbFeBr_3$ side of the phase diagram, closer to the parent compound with larger induced moment.

The bulk magnetic behaviour of the compounds $RbFeCl_{3-x}Br_x$ ($x = 1.0, 1.5, 2.0$ and 3.0) has been studied at the Gorlaeus Laboratories, University of Leiden, using single-crystal DC magnetic susceptibility measurements over the temperature range 2–120 K and by magnetisation measurements at 2 K in fields of up to 5.6 T (Visser 1988a).

The magnetic susceptibility behaviour is similar to that measured in the pure compounds $RbFeCl_3$ (Eibschutz *et al* 1975) and $RbFeBr_3$ (Lines and Eibschutz 1975). The susceptibility perpendicular to the c axis, $\chi^{\perp}$, was found to vary linearly with composition over the range $1.0 < x < 3.0$. For all the mixed compounds no evidence has been found for magnetic long-range order. The magnetic susceptibility along the c axis, $\chi^{\parallel}$, showed a maximum at T_{max} for all compositions; the position of this maximum increased from

11 to 13.5 K for $x = 0$ to $x = 3.0$. For compositions $1.5 < x < 3.0$ the overall magnetic exchange was found to be antiferromagnetic as indicated by the plots of $1/\chi^{\parallel}$ against T. The sign of the exchange for $x = 1.0$ could not be determined with much confidence, so this compound appears to lie near the crossover from ferro- to antiferromagnetic intrachain exchange.

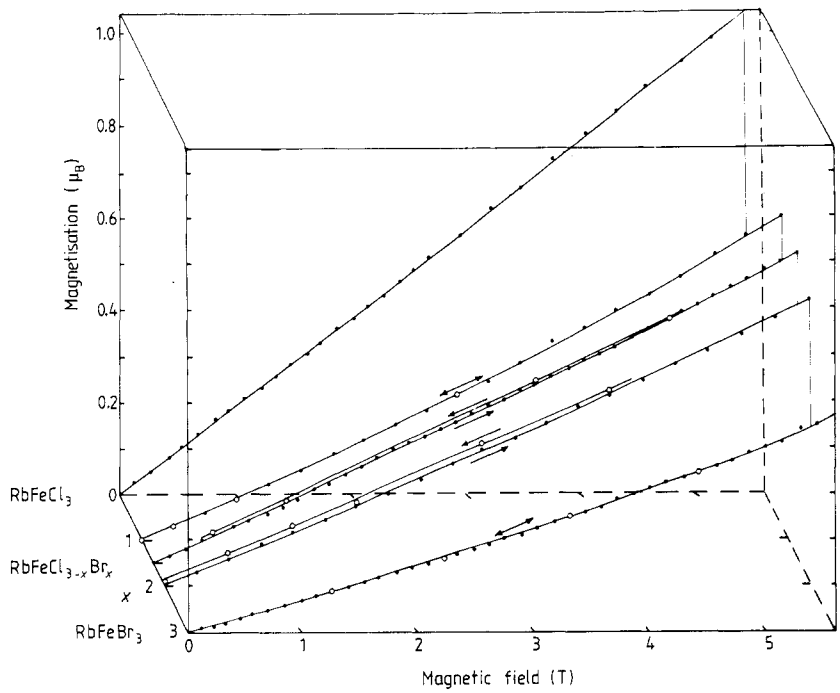

Figure 2. Magnetisation curves for the mixed system $RbFeCl_{3-x}Br_x$ with the field applied parallel to the crystal c axis at 2.0 K for various compositions ($x = 0$, 1, 2 and 3). The full circles denote measurements taken as the field was increased and the open circles those taken on reducing the field. The lines drawn through the points merely provide a guide to the eye.

The magnetisation data at 2.0 K with a magnetic field of 5.6 T show that the components of the induced moment parallel and perpendicular to the crystal c axis vary smoothly with composition over the range $1.0 < x < 3.0$. The magnetisation curves show remanent magnetic behaviour for the compound $RbFeClBr_2$ and to a lesser degree for the compound $RbFeCl_{1.5}Br_{1.5}$ (figure 2). No remanent effects could be detected at lower values of x or for pure $RbFeBr_3$ or $RbFeCl_3$. Similar remanent behaviour has been observed in a wide range of spin-glass or semi-spin-glass compounds (Hubsch and Gavoille 1982, Grest and Soukoulis 1983).

Thus, we have performed single-crystal neutron diffraction on samples with *higher* ($x > 2.7$) or *lower* ($x < 0.3$) values of x than used previously to study the effect of small amounts of dopant on the magnetic structure of the pure compounds. In addition, we have measured the diffuse scattering from samples of intermediate compositions to try to deduce the nature of any short-range magnetic correlations.

2. Experimental details

Stoichiometric amount of 'ultrapure'-grade (purity >99.99%) RbCl and RbBr, obtained from Alfa Inorganics, Ventron Ltd, were melted with sublimed $FeCl_2$ and $FeBr_2$ in sealed silica ampoules. The $FeCl_2$ had been prepared from the Analar-grade hydrate, $FeCl_2 \cdot 4H_2O$, by heating to 700 °C in a stream of dried nitrogen and HCl gas; $FeBr_2$ was prepared at 700 °C by passing HBr and nitrogen gas over iron powder, purchased from Goodfellow Metals Ltd, at 99.99% purity. Single crystals of these mixtures were grown by the Bridgman method by pulling the ampoules at 1.2–1.5 mm h^{-1} in a Crystalox twin-zone Bridgman furnace.

To determine the compositions of the $RbFeCl_{3-x}Br_x$ samples used in the neutron diffraction experiments we analysed pieces taken from different regions of the same boule by argentimetric titration and x-ray microprobe analysis (Cheetham and Skarnulis 1981). Both methods indicated that the samples used in the diffraction measurements were homogeneous to within 1% of the total halide content, i.e. in the case of boules with nominal chloride contents of 14% and 2% the analysis revealed 14 ± 1% and 2 ± 1% chloride respectively.

Samples, typically measuring 3 × 3 × 5 mm^3, were cleft from the boules. Crystals rich in $RbFeBr_3$ were mounted with the $(002)_N$ and $(220)_N$ reflections in the horizontal scattering plane, while those rich in $RbFeCl_3$ or intermediate in composition were mounted with the $(100)_N$ and $(220)_N$ reflections in the scattering plane. Neutron diffraction experiments were performed on single crystals of $RbFeCl_{3-x}Br_x$ (where x = 0.03, 0.06, 0.15, 2.58, 2.76 and 2.94) using the two-axis diffractometer D15 at the Institut Laue–Langevin (ILL), Grenoble. The neutron wavelength was 1.174 Å and collimation before and after the sample was provided by two sets of apertures measuring 12 mm square and set at 10 cm from the sample. The divergence of the neutron beam was 1° at the sample. A tilting counter allowed the scattered neutron intensity to be mapped in the $l = 0$ plane as well as parts of the $l = 1$ plane while the sample remained fixed with the c axis vertical. Temperatures down to 1.3 K were provided by an ILL 'Orange' cryostat. The scattered neutron intensity was mapped as a function of temperature in the regions of the K point and the M point of the hexagonal reciprocal lattice. These maps consisted of a series of parallel scans centred on and perpendicular to the $[1\,1\,0]_N$ direction. Further scans were made along the high-symmetry directions KM and KΓ in the Brillouin zone. For crystals in which no scattering maxima were found in the $l = 0$ or $l = 1$ planes, scans were made parallel to the c axis, cutting the $l = 0$ or $l = 1$ planes at $\boldsymbol{Q} = (0.30.3l)_N$. Such measurements probed the form of any one-dimensional magnetic short-range order.

3. Results

3.1. Data analysis procedure

The elastic neutron scattering lineshapes in reciprocal space are proportional to the Fourier transform of the static spin pair-correlation function. In solids which have magnetic long-range order this results in δ-functions in reciprocal space, and scattering profiles that are equal to the instrumental resolution function, generally taken to be a Gaussian curve. For inhomogeneous magnets there are two common forms that the

resolution-corrected lineshape may take. Dilute magnets in the absence of a magnetic field usually show a Lorentzian lineshape that arises from an exponential decay of the spin correlation function in real space. In the presence of random magnetic fields—which may be produced either by applying a magnetic field to a dilute Ising antiferromagnet or in a body of ferromagnetically correlated moments containing frozen moments of random orientation—a distinct Lorentzian-plus-Lorentzian-squared lineshape is seen (Birgeneau *et al* 1984). Thus, a plot of log I against log($|\boldsymbol{q}|$) (where I is the neutron scattering intensity at a wavevector $\boldsymbol{q}$ from the scattering maximum) should be a straight line with a gradient between 2 and 4. Finally, it should be noted that a different form of lineshape has been seen in the quadrupolar glass $(KBr)_{1-x}(KCN)_x$ (Loidl *et al* 1985). There, the dependence of I on $|\boldsymbol{q}|$ may be divided into a term proportional to q^{-2} and a term proportional to q^{-1}. Contours of equal intensity drawn in reciprocal space were also found to be very anisotropic. The origin of this effect is uncertain and has been proposed to arise from randomly distributed mechanical strains caused by the chemical disorder. Similar behaviour has been seen in the randomly mixed ferroelectric–antiferroelectric compounds $Rb_{1-x}(NH_4)_xH_2PO_4$ (Hayase *et al* 1985).

The data were corrected for background scattering measured for each sample at 6 or 20 K. The remaining intensity was then least-squares-fitted to the lineshape functions described in the previous paragraph, i.e. to the pure Gaussian resolution function or to Lorentzian or Lorentzian-plus-Lorentzian-squared lineshapes convoluted with the instrumental resolution function. In all the cases where $x < 0.15$ an ω (tangential) scan through the nuclear Bragg peaks revealed a symmetric lineshape whose form was very close to that of a Gaussian curve. The resolution function of the instrument was derived from the width of the magnetic Bragg peak at the K point of a sample of $RbFeCl_3$ which had nuclear peak widths within 10% of the compounds with low x. It was found that the scattering from samples with $x = 0.06$ and 0.15 was much better described by a Lorentzian curve convoluted with the instrumental resolution function compared with a Gaussian curve: χ^2 for the fits generally lay between 1 and 2, improving by only 0.05 on the inclusion of an additional Lorentzian-squared component.

It was not possible to assign a lineshape unambiguously to the scattering from samples rich in $RbFeBr_3$ ($x > 2.58$) since they possessed broad, asymmetric nuclear and magnetic Bragg reflections (typically 0.7° at $|\boldsymbol{Q}| = 1.2$ Å^{-1}, where $|\boldsymbol{Q}| = 4\pi(\sin\theta)/\lambda$) compared with the narrower, symmetric reflections from samples rich in $RbFeCl_3$ (typically 0.3° at the same value of $|\boldsymbol{Q}|$).

In addition to the distinct peaks at the K point or at the incommensurate satellite positions a broad, diffuse peak was seen that was centred at the K point. An example is given in figure 3. The background scans along the KM direction for the $x = 0.03$ and $x = 0.06$ samples were taken at a maximum temperature of 6 K. Careful peak fitting revealed a broad maximum centred at the K point at this temperature. A similar, though more distinct, maximum was observed at the same temperature in a sample of $RbFeCl_3$ doped with 2% of the diamagnet $RbMgCl_3$ (Harrison and Visser 1988b), but was found to have disappeared at 20 K. We conclude that the 6 K scans are invalid for the purpose of background correction. The scan depicted in figure 3 was taken at 1.6 K through $(\frac{1}{3}\frac{1}{3}0)_N$ in a direction perpendicular to $[110]_N$. It was corrected for background scattering measured at 20 K and clearly reveals scattering intensity in addition to a strong Gaussian or Lorentzian central component. Similar values of χ^2 were obtained for fits to a Lorentzian curve convoluted with the instrumental resolution function, describing the diffuse component, and either a pure Gaussian curve or a Lorentzian curve convoluted with the instrumental resolution function describing the sharper peak. The latter was

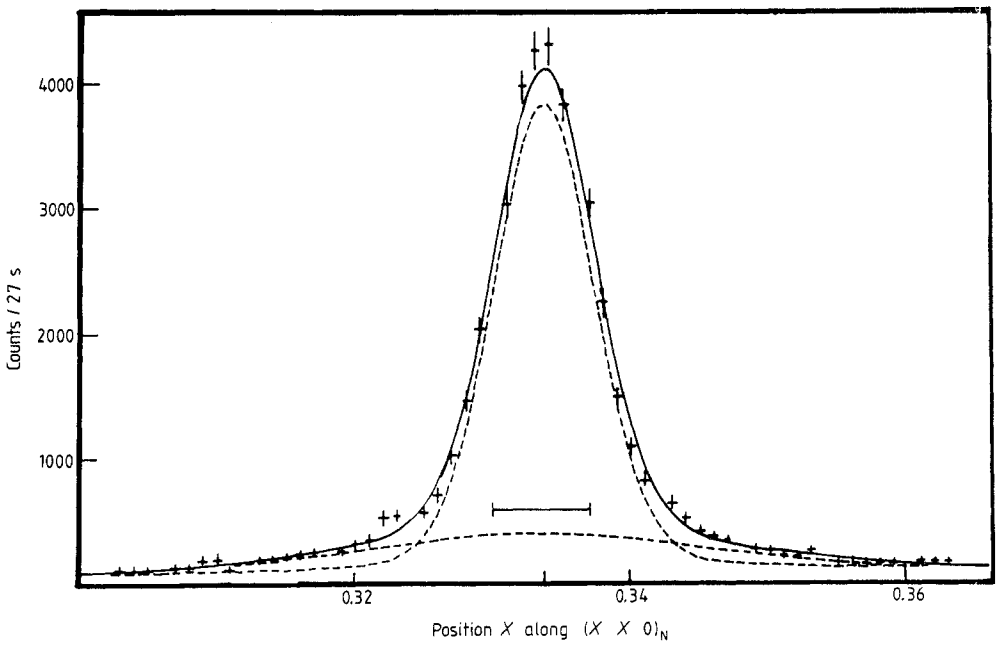

Figure 3. Neutron scattering profile at $(\frac{1}{3}\frac{1}{3}0)_N$ for the $x = 0.03$ sample at 1.6 K. The scan was taken in a direction perpendicular to $[1\,1\,0]_N$ and corrected for background scattering taken at 20 K. The full curve through the points is the least-squares-fitted sum of a sharp and a broad Lorentzian curve convoluted with the instrumental resolution function. The resolution width at this point is denoted by a horizontal bar at the centre of the peak.

preferred to the former on the grounds that the reflection is slightly wider than the resolution width. This apparent broadening could arise from errors in the estimate of the resolution width. Consequently, the resolution-corrected peak widths for the scattering maxima in $RbFeCl_{3-x}Br_x$ could be significantly smaller than those displayed later in figure 8 and should be treated with caution.

The intensities of the magnetic scattering from each sample, scanned perpendicular to the $[1\,1\,0]_N$ direction, were normalised to the intensities of their respective $(1\,1\,0)_N$ reflections. These in turn had to be corrected for the change in structure factor, $F_{110}(x)$,

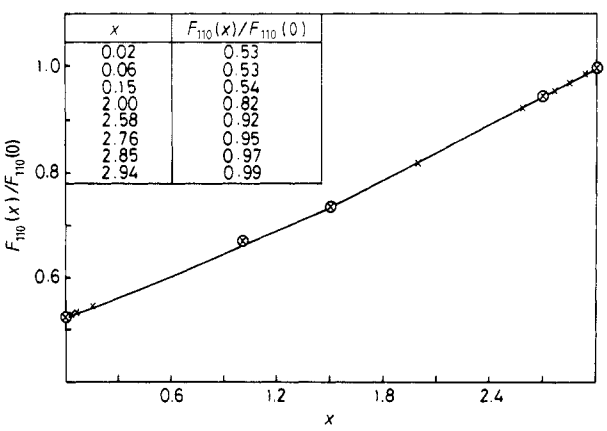

Figure 4. The dependence of the structure factor of the $(110)_N$ reflection in $RbFeCl_{3-x}Br_x$ on composition x at 1.3 K. Experimental values were calculated from the powder neutron diffraction data of Visser and Harrison (1982), and are denoted by crosses in circles. An arbitrary curve has been drawn through these points to obtain values of $F_{110}(x)$ for the values of x possessed by the samples used in the single-crystal work. These are denoted by crosses alone.

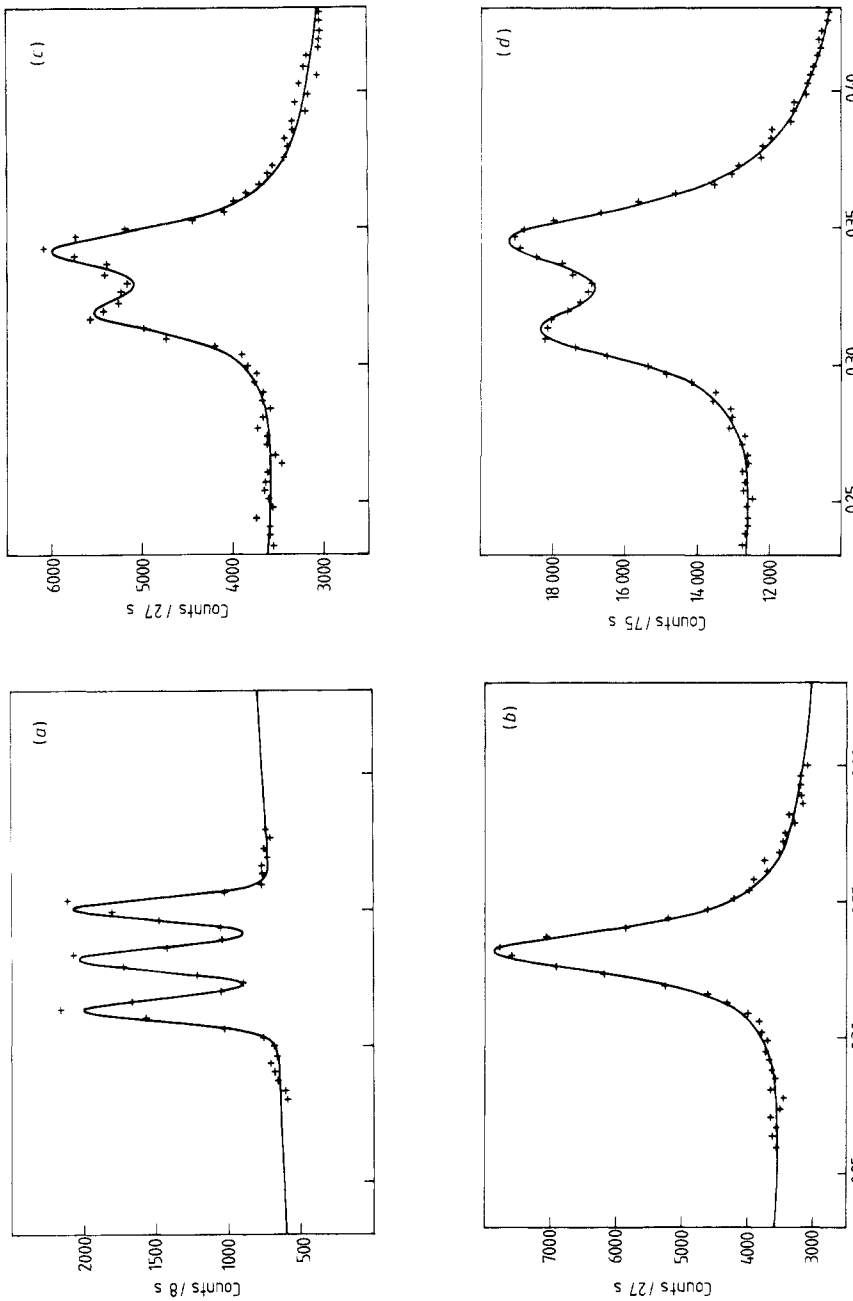

Figure 5. Examples of single-crystal neutron scattering data for: (*a*) pure $RbFeCl_3$ at 2.07 K; (*b*) and (*c*) the $x = 0.03$ sample at 1.65 and 1.83 K respectively; (*d*) the $x = 0.06$ sample at 1.38 K. These data have not been scaled against the relative intensities of the $(1\,1\,0)_N$ reflections, nor have they been corrected for background scattering. All scans were taken along the KM direction, through the K point. The axis label X is thus the position along KM: $(X\,\frac{1}{2} - \frac{1}{2}X\,0)_N$.

which depends on the composition x on account of the difference in the scattering lengths of Br and Cl, and the change with composition of the average position of the halide ion within the unit cell. A value for the latter was taken from the powder diffraction measurements of Visser and Harrison (1982) on a wide range of $RbFeCl_{3-x}Br_x$ compounds at 1.3 K. The results are displayed in figure 4, which was used to scale the intensities of the $(1\,1\,0)_N$ reflections of the present set of samples.

3.2. Neutron scattering from samples with small concentrations of impurities ($x \leqslant 0.15$ and $x \geqslant 2.76$)

On the $RbFeCl_3$ side of the phase diagram we observed narrow neutron scattering intensity maxima at the positions of the magnetic Bragg peaks of pure $RbFeCl_3$ (figure 5). The magnetisation curves for crystals of composition $x = 0.03$, 0.06 and 0.15, measured at $(\frac{1}{3}\frac{1}{3}0)_N$, are displayed in figure 6(*a*). The curve for pure $RbFeCl_3$, measured on the same instrument at the same wavelength, is included for comparison. These data have all been normalised to the relative intensities of their $(1\,1\,0)_N$ reflections as described in the previous section.

Correlations corresponding to the C phase of pure $RbFeCl_3$ were only observed at the lowest experimental temperature for the $x = 0.03$ sample. At higher T or larger values of x the scattering intensity was much lower and one only saw the satellite peaks arising from the IC_1 and IC_2 type magnetic correlations. The displacement of the satellite peaks from the K point, δR, increased with temperature and dopant concentration as depicted in figure 7. The value of the maximum displacement is independent of dopant concentration as is the temperature at which the magnetic scattering near the K point

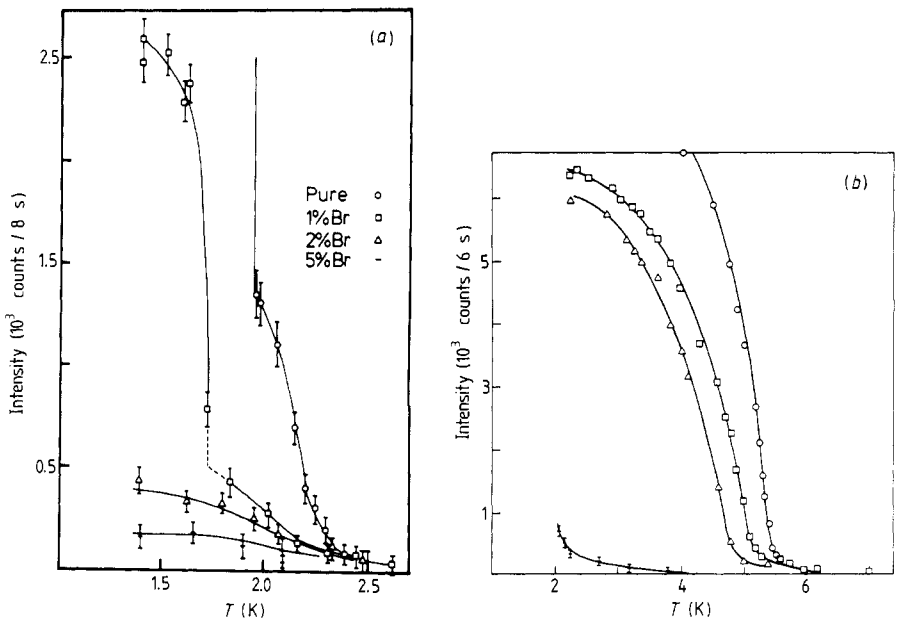

Figure 6. The temperature dependence of the integrated scattering intensity for (*a*) small values of x, measured at the K point, and (*b*) large values of x, measured at the H point. All data have been scaled against the relative intensities of the nuclear (110) and (220) reflections.

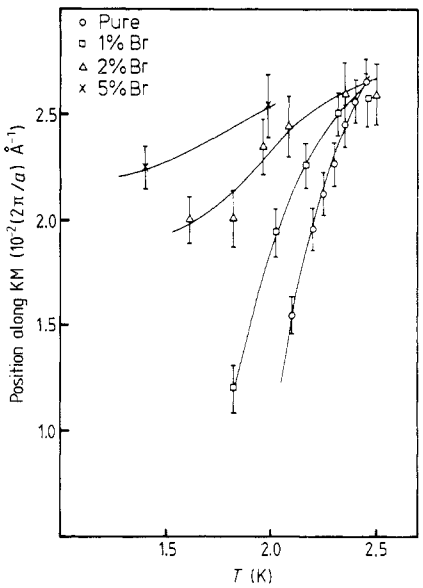

Figure 7. The displacement δR from the K point of the magnetically scattered neutron intensity maxima for samples of composition $x = 0.03, 0.06$ and 0.15. Values for pure $RbFeCl_3$ measured on the same instrument have been added for comparison.

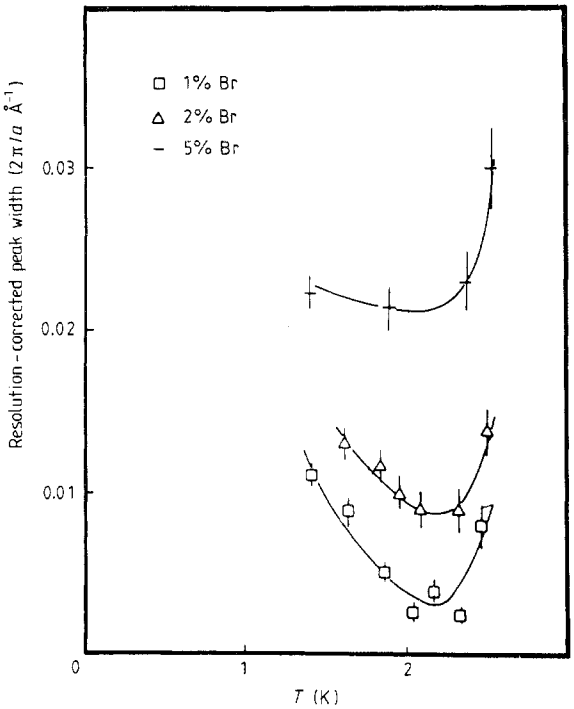

Figure 8. The dependence of the resolution-corrected peak width on temperature and composition for samples of composition $x = 0.03, 0.06$ and 0.15. The peak in question is the distinct peak at the K point. Note that the data for $x = 0.03$ depend very much on our estimate of the resolution width, the uncertainty in which is not accounted for in the error bars on the data points.

tended to zero, remaining at 2.5 ± 0.1 K. A similar result was found for $Rb_{1-x}Cs_xFeCl_3$ (Harrison *et al* 1986a) and $RbFe_{1-y}Mg_yCl_3$ (Harrison and Visser 1988b).

The Lorentzian peak width *always* increased with dopant concentration. The widths of the magnetic Bragg peaks of $RbFeCl_3$ remained strictly resolution-limited throughout the IC_1, IC_2 and C phases, but those for crystals of composition $x = 0.03$, 0.06 and 0.15 appeared to pass through a minimum at about 2.1 K (figure 8).

In addition to the relatively distinct features noted above, all the doped samples on the $RbFeCl_3$ side of the phase diagram showed a diffuse peak centred at the K point (figure 3). We cannot be very explicit about the nature of this peak for two reasons. First, for the $x = 0.15$ crystal, and to a lesser extent for the $x = 0.06$ crystal, the diffuse character of the principal peaks made them very difficult to resolve from this secondary feature. Secondly, the background scans along the KM direction for the $x = 0.03$ and $x = 0.06$ crystals were not at a sufficiently high temperature for them to be valid (see § 3.1). The scan of figure 5, which was adequately corrected for background scattering, is the only one taken in the $[1\bar{1}0]_N$ direction, through the K point. However, it *is* possible to deduce from the data that for crystals of composition $x = 0.03$ and 0.06 the diffuse component became broader and more intense as the temperature was raised and it persisted to at least 6 K. The magnetic correlation length in the *ab* plane of the $x = 0.03$

sample appeared to be approximately $16a$ at 2.02 K and about $5a$ at 2.9 K, where a is a unit-cell parameter.

Turning now to samples on the $RbFeBr_3$ side of the phase diagram, we also observed narrow neutron scattering intensity maxima at the positions of the magnetic Bragg peaks of pure $RbFeBr_3$. The magnetisation curves for crystals of composition $x = 2.94$, 2.85 and 2.76 are shown in figure 6(b). The measurements were made at the H point ($\boldsymbol{Q} = (\frac{1}{3}\frac{1}{3}1)_N$ and the intensities were normalised to the relative intensities of the $(110)_N$ reflections. Poor crystal quality invalidated attempts to assign a lineshape to the peaks; both the nuclear and the magnetic reflections increase in width with the proportion of $RbFeCl_3$ present.

A possible explanation for the large mosaic spread and poor crystal quality at high values of x may be found in the structural phase transition of $RbFeBr_3$. The electron diffraction measurements of Visser and Prodan (1980) showed that this type of structural phase transition in ABX_3 compounds from $P6_3/mmc$ to $P6_3cm$ symmetry is accompanied by a large increase in structural disorder. The introduction of small amounts of Cl^- to $RbFeBr_3$ may help to trigger such disorder by acting as nucleating points for structural domains. The $P6_3/mmc$ lattice of $RbFeCl_3$ does not appear to be so susceptible towards distortion.

The crystals with $x = 0.06$ and 0.15 showed distinct maxima in the neutron scattering intensity at the H point ($\boldsymbol{Q} = (\frac{1}{3}\frac{1}{3}1)_N$) but the $x = 0.24$ sample only showed a broad weak maximum at this position at temperatures down to 2.07 K. However, the temperature dependence of the integrated intensity shows a sharp increase near 2.1 K, implying

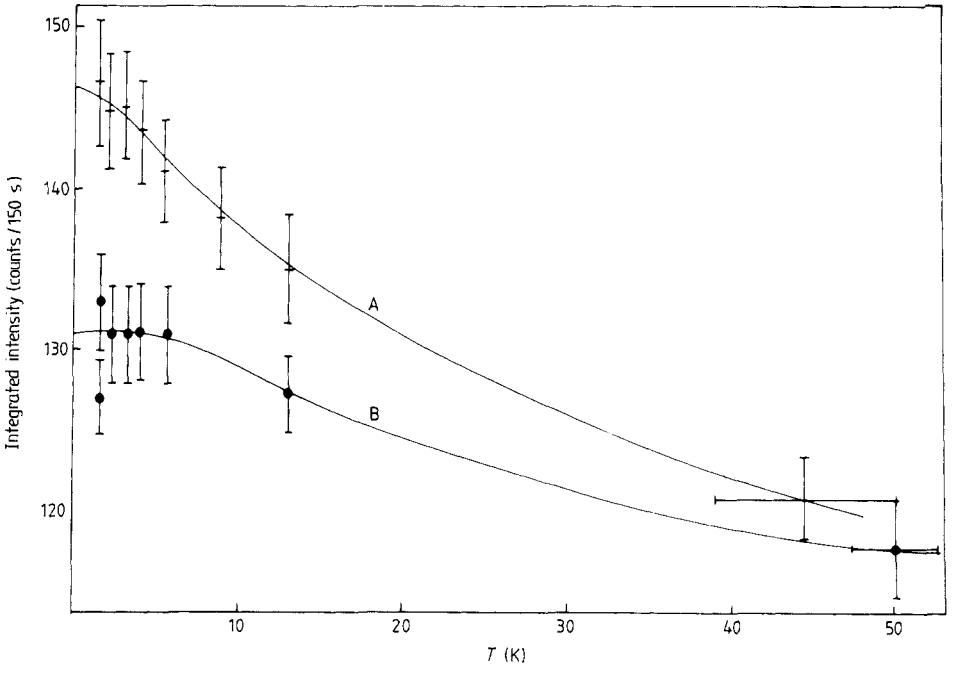

Figure 9. The dependence on temperature of the magnetically scattered neutron intensity in the $l = 1$ plane centred at $\boldsymbol{Q} = (0.60.61)_N$ (curve A) and $\boldsymbol{Q} = (\frac{1}{3}\frac{1}{3}1)_N$ (curve B). The data were collected by making scans parallel to the crystal c axis from $l = 0.7$ to $l = 1.3$. No background correction has been made to these data.

either a rapid increase in the magnetic correlation length or an increase in the magnitude of the magnetic moment (figure 6(*b*)).

3.3. Neutron scattering from samples with high concentrations of impurities (0.15 < x < 2.76)

The $x = 2.76$ crystal represents a borderline case, showing some evidence for the onset of long-range order at about 2.1 K. The $x = 2.58$ crystal, however, showed no maximum when scanned within the $l = 1$ plane near the H point. A scan perpendicular to the $l = 1$ plane, cutting it at $\boldsymbol{Q} = (\frac{1}{3}\frac{1}{3}1)_N$ or $\boldsymbol{Q} = (0.60.61)_N$, displays a broad maximum in the scattering intensity at $l = 1$. The dependence on temperature of this intensity is shown in figure 9.

The crystal of $RbFeCl_2Br$ ($x = 1.0$) showed no maximum at all in the scattered neutron intensity when scanned parallel to the crystal c axis through the $l = 0$ or $l = 1$ planes and cutting them at $(0.10.1l)_N$, using a counting time as long as 5 min/point at temperatures down to 1.6 K.

4. Discussion

4.1. The magnetic structure of $RbFeCl_{3-x}Br_x$ for small concentrations of dopant ($x \leq 0.15$ and $x \geq 2.76$)

4.1.1. The effect of dopant on the magnetic ordering temperatures. Very low concentrations of either type of dopant destroys the magnetic long-range order of the majority component. $RbFeBr_3$ is more resilient towards this effect than $RbFeCl_3$ as would be expected of the compound with the larger induced moment and the higher value of T_N.

The mixing of $RbFeCl_3$ and $RbFeBr_3$ in any proportion introduces randomness in J_1, J_2 and D as a result of the delicate balance between the local crystal structure and the magnetic parameters of these materials. There are many examples in the literature of models that treat disorder in any one of these magnetic parameters but there does not seem to be a model that embraces all of these sources of disorder to produce a net result. The effect of diamagnetic impurities of randomness in intra-chain exchange on the magnetic ordering in classical Heisenberg or Ising chains weakly coupled by a molecular field was modelled by Hone *et al* (1975). This model has enjoyed considerable success in describing the effect of diamagnetic impurities on the Néel temperature of the ferromagnetic linear-chain compound $CsNiF_3$ (Steiner and Axmann 1976) as well as antiferromagnetic linear-chain compounds such as TMMC (Takeda and Schouten 1981 and references therein). In these cases the ratio J_2/J_1 is small (10^{-2}–10^{-4}).

In figure 10 we plot the predictions of the Hone model for the dependence of the ordering temperature of $RbFeCl_3$ and $RbFeBr_3$ on diamagnetic impurity concentration. It has been assumed that both magnets have Heisenberg symmetry and spin $S = 1$. The different values for J_1 and J_2 are taken from table 2 and result in two different predicted dependences of T_N on dopant concentration. It is clear that the measured fall-off of T_N with dopant concentration is much faster than that calculated here. It is also clear that there are several difficulties in implementing the Hone model in the present case.

First, it is not obvious how one should relate the concentration of Br^- ions to the concentration of either site or bond impurities in the Hone model. This would require a microscopic understanding of the exchange in the intra-chain bridges containing mix-

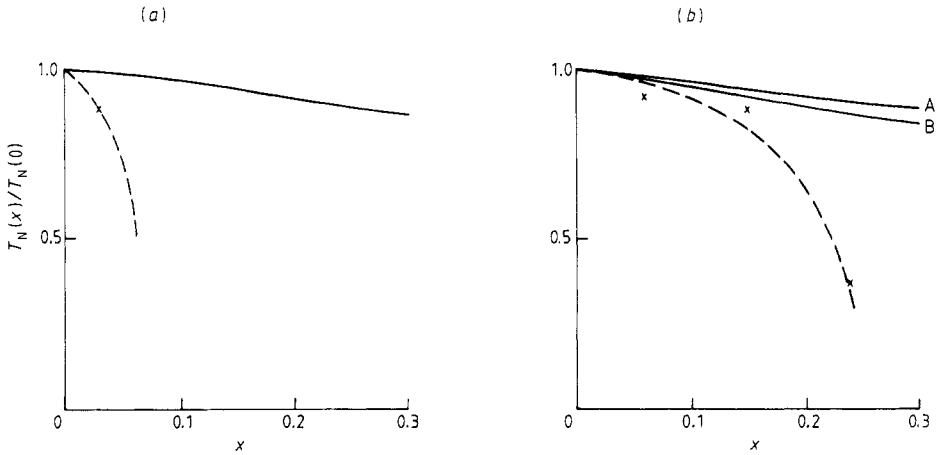

Figure 10. The dependence of the ordering temperature of (*a*) $RbFeCl_3$ and (*b*) $RbFeBr_3$ on concentration of impurity. The points plotted as crosses are experimental values for T_N taken from the present work and the full curves represent the predictions of the Hone model for diamagnetic impurities in a Heisenberg magnet. The broken curves drawn through the experimental points are merely a guide to the eye. In case (*a*) the ordering temperature is taken as the C–IC$_1$ transition temperature. The values for exchange constants are taken from table 2. In case (*b*) there are two ratios of J_1/J_2 that could be chosen: values taken from the data of Lines and Eibschutz (1975) are used for curve A and those from Harrison and Visser (1988a) for curve B.

tures of halide ions. Secondly, the $RbFeCl_{3-x}Br_x$ system cannot be treated as an assembly of classical moments. Molecular-field calculations are not suitable for the treatment of induced-moment magnets that are close to the magnetic singlet ground-state threshold. Thirdly, it is not certain what value we should take for $T_N(x)$ or even for $T_N(0)$: the added influence of the large magnetic dipole–dipole interaction on the ordering process obscures the value of T_N that would arise from just the superexchange interactions, as modelled by Hone *et al* (1975). It should be noted that the Hone model is best applied to magnets for which $J_2/J_1 \ll 1$. This ratio appears to range from 10^{-1} to 10^{-2} for $RbFeCl_3$ and $RbFeBr_3$ according to the values given in table 2 and this may limit the accuracy of the model. It should also be noted that the single-ion anisotropy D, which is neglected in the Hone model, may also be important. It has been shown that the inclusion of D in the calculation of T_N of undiluted one-dimensional magnets has a significant effect (Boersma *et al* 1981).

Existing theories that treat randomness in D are also not appropriate in the present case, being concerned either with mixtures of magnets with Ising and XY anisotropies (Bevaart *et al* 1978, Wong *et al* 1980, Katsumata *et al* 1982), or with cases in which D is uniaxial and constant in magnitude but in which the direction of the anisotropy axis varies with site (Rhyne *et al* 1972, Kettler *et al* 1981). In the case of $RbFeCl_{3-x}Br_x$ the sign of D remains the same; it is XY in character throughout and has a magnitude that we expect to vary only weakly with composition (compare the values of D for the two pure compounds in table 2).

A quantitative interpretation of our results may only be obtained from a very specific model, designed to meet all the peculiarities of the present system. Thus we shall only attempt a qualitative explanation by considering the effect of dopant on the ratio D/J_Q.

It is likely that J_1 is reduced or made negative by the replacement of one or two

chloride ions by bromide ions in the intra-chain exchange bridges. It is also probable that J_2 is increased in magnitude on replacing Cl^- by Br^- in the inter-chain exchange bridges. This is expected to be a less important effect than that concerning J_1 because the values of J_2 for the chloride and bromide are close in value (Harrison and Visser 1988a), and J_2 is smaller than J_1 by a factor of 5–10. Thus, in the vicinity of Br^- ions in $RbFeCl_3$, J_Q (where $Q = (\frac{1}{3}\frac{1}{3}0)_N$) will also be reduced, and a lowering in size of the neighbouring magnetic moments will occur. The proximity of the magnetic–singlet ground-state threshold will sensitise the reduction of the magnetisation by impurities, making it more severe than would be predicted from molecular-field arguments. On this basis the ordering temperature of $RbFeBr_3$ is expected to be less sensitive towards dopant than that of $RbFeCl_3$. This is consistent with our results (Figure 10).

Finally, it should be noted that the magnetic inhomogeneities not only reduce T_N but also destroy the long-range character of the magnetism in the 'ordered' magnetic phases for $x < 0.15$. No clear explanation of this phenomenon can be found in the literature. It has been stated that small concentrations of impurities in a frustrated two- or three-dimensional lattice of moments with spin dimensionality $n \geqslant 1$ at $T = 0$ give rise to random magnetic fields that destroy the magnetic long-range order (Matsubara 1985).

4.1.2. The effect of dopant on the balance between magnetic dipolar and superexchange ordering. Let us now consider the effect of doping $RbFeCl_3$ with $RbFeBr_3$ on the balance between the magnetic dipole–dipole interaction γ and J_2. Several effects must be considered. First, the reduction or elimination of magnetic moments at the iron sites will reduce the magnitude of *both* γ and J_2. Intuitively one might expect that the longer-range dipolar interaction would be disrupted less by reduction of moments at random sites. Secondly, the replacement of Cl^- by the more covalent Br^- is likely to increase J_2 (compare the values of J_2 for the pure compounds in table 2). Finally, the substitution of Br^- ions into the chains reduces the intra-chain ferromagnetic interactions, which in turn reduce γ.

There is no ready way in which the net result of these competing effects may be assessed theoretically. Experimentally, the ratio γ/J_2 appears to increase on doping $RbFeCl_3$ with $RbFeBr_3$: doping has little effect on the P–IC_1 transition temperature and the C–IC_2 transition temperature falls with dopant concentration (figure 11); the displacement from the K point, δR, of the satellite peaks in the IC phases at a particular temperature increases with dopant concentration.

On comparing figure 7 with figure 4 of Harrison *et al* (1986a) we see that the displacement of the satellite peaks from the K point is smaller at a given temperature and impurity concentration for the bromide- than for the caesium-doped materials. This indicates that doping with Cs^+ favours γ/J_2 more than doping with Br^-. In some respects the effect of Cs^+ on the ratio γ/J_2 should be similar to that of Br^-. The reduction or elimination of magnetic moments close to Cs^+ impurities throughout the crystal reduces both γ and J_2. However, Cs^+ is expected to have a different effect on J_2 than Br^-. The larger Cs^+ ion ($r_{Cs} = 2.00$ Å) pushes the iron chains further apart than those in pure $RbFeCl_3$ ($r_{Rb} = 1.85$ Å). The value of γ depends on inter-chain separation r as r^{-3} whereas the dependence of J_2 on r is of the order of r^{-10} (Bloch 1966). Bromine ions will also cause the iron chains to be displaced further than in pure $RbFeCl_3$ but this is offset by the increase in the covalency of the inter-chain exchange bridges, leading to an increase in J_2 from the chloride to the bromide (table 2). Furthermore, the bromide ion is more polarisable than the Cs^+ ion and should be more easily accommodated in the $RbFeCl_3$ lattice causing less local structural distortion.

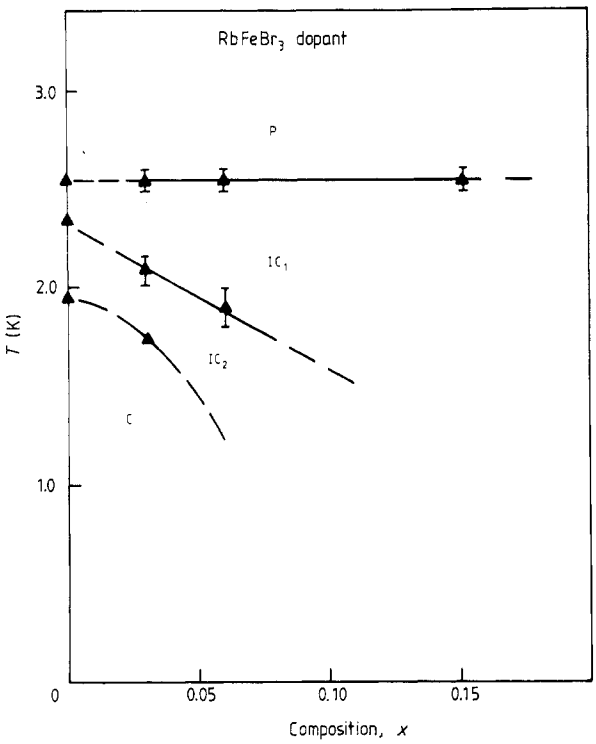

Figure 11. The dependence on temperature and concentration of Br^- of the periodicity of the magnetic correlations in $RbFeCl_3$. The magnetic correlations are finite in extent so that these phases differ from those found in the pure chloride—hence the broken curves extrapolated to zero impurity level. Symbols IC_1, IC_2 and C refer to the incommensurate and commensurate periodicities predicted by Shiba (1982). The two lower phase boundaries were not seen down to the base temperature of 1.3 K for the $x = 0.15$ sample, so again the phase boundary is drawn as a broken line.

4.2. Diffuse magnetic scattering from $RbFeCl_{3-x}Br_x$ ($0 < x \leq 0.15$ and $2.76 \leq x < 3.0$)

A diffuse neutron scattering component is seen in samples rich in $RbFeCl_3$ ($x < 0.15$), in addition to the relatively narrow intensity maxima seen near the K point below 2.5 K. Only one scan ($x = 0.03$ at 1.6 K) containing information about this feature could be corrected for background scattering. The diffuse scattering profile could be fitted to a Lorentzian curve of width $(\pi/25a)$ $Å^{-1}$, where a is the nuclear unit-cell parameter. There are several interpretations that may be given to this feature.

(i) Scattering arises from small ($\simeq$50 Å diameter) magnetically ordered clusters with a 120° antiferromagnetic configuration in the *ab* plane.

(ii) The magnetically ordered regions are large but the orientation of the moments adopts a distribution of canting angles which is centred on the 120° antiferromagnetic array. When inhomogeneities are introduced to a triangular antiferromagnetic array of moments the balance of force producing the 120° Néel ground state is broken and the formation of 'canted local states' is expected (Villain 1979, Harrison 1987). Significant canting about a single impurity may extend over several neighbouring shells of moments, setting up a medium-range magnetic disordering potential. Interactions between such centres occurs through polarisation of the intervening medium, and may lead to semi-spin-glass formation (Villain 1979). In that case a longitudinal lattice or sublattice magnetisation co-exists with a random transverse lattice or sublattice magnetisation. The one-dimensional antiferromagnet $CsMnBr_3$ undergoes three-dimensional magnetic long-range order to produce a 120° antiferromagnetic array in the *ab* plane and this material also shows diffuse neutron scattering about the H point ($\boldsymbol{Q} = (\frac{1}{3}\frac{1}{3}1)$) when doped with diamagnetic (Mg^{2+}) or magnetic (Fe^{2+}) impurities (Visser and McIntyre

1988, Visser *et al* 1988). Another reason that the moments may deviate from the ordered 120° antiferromagnetic array is that they may lie at the boundary between two magnetic domains.

An additional source of diffuse magnetic scattering may be present in $RbFeBr_3$. A recent specific-heat study of this material (Adachi *et al* 1983) showed that it orders in two steps: there is a sharp specific-heat anomaly at 5.5 K and a broad, weak one at 2.0–2.5 K. The phase that exists between these two anomalies has been postulated to be a partially ordered one in which one of the three magnetic chains in the $a\sqrt{3} \times c$ unit cell is disordered. Similar partially disordered magnetic phases have been observed in the 1D Ising system $CsCoCl_3$ (Mekata *et al* 1986). They have also been proposed as an explanation for the diffuse neutron scattering observed in the powder diffraction patterns of undoped samples of the two-dimensional triangular Heisenberg antiferromagnets VCl_2 and VBr_2 below T_N (Hirakawa *et al* 1983). At 2.5 K the third chain in $RbFeBr_3$ orders to give a slightly modified 120° degree structure (Adachi *et al* 1983). However, the scattering from the disordered chain should merely contribute to the magnetic diffuse scattering background in an isotropic fashion within $l = 2n - 1$ planes in reciprocal space. As the temperature falls below that of the second ordering transition this diffuse intensity should condense at the magnetic Bragg positions, increasing their intensity by 50%. It should be noted that our measurements do not provide any evidence for such an ordering sequence.

A modification of this ordering process is expected in pure $RbFeBr_3$ and samples of $RbFeCl_{3-x}Br_x$ of composition $x > 2.76$. The structural phase transition that creates two nuclear sublattices, A and B, as described in § 1.2, gives rise to different inter-chain exchange constants, J_{A-B} and J_{B-B} (where the subscript describes the sublattice to which each moment belongs). This will upset the balance of forces that leads to the 120° antiferromagnetic array when J_2 is uniform in the *ab* plane and pin the mobile character of the triangular antiferromagnetic array.

4.3. Magnetic ordering behaviour of $RbFeCl_3$ at intermediate compositions ($0.15 > x > 2.76$)

The neutron scattering measurements clearly demonstrate that the $x = 2.56$ crystal has significant one-dimensional antiferromagnetic correlations at 1.6 K and that the $RbFeCl_2Br$ crystal ($x = 1.0$) has no detectable long-range ferro- or antiferromagnetic intra-chain correlations at the lowest experimental temperature for this sample of 1.6 K.

The magnetisation and susceptibility measurements (see § 2.2) shed more light on these observations.

(i) The magnitude of the induced magnetisation and of the maximum magnetic susceptibility parallel to the crystal *c* axis dropped from $RbFeCl_3$ to $RbFeBr_3$, reflecting the transition from ferro- to antiferromagnetic J_1. The drop in the susceptibility was most marked between $x = 0.0$ and $x = 1.0$. This crossover is illustrated schematically in figure 12(*a*). At a microscopic level we expect there to be a distribution of compositions of magnetic exchange bridges and consequently a distribution of values of the individual intra-chain exchange constant, J_{1i}. For individual bridges for a particular impurity concentration x. This is illustrated schematically in figure 12(*b*). Note that J_{1i} appears to have a continuous range of values for a given x despite there being only four different types of Fe–X_3–Fe bridge. This is because J_{1i} is very sensitive to structural distortions and therefore also depends on the distribution of other neighbouring halide ions. Note

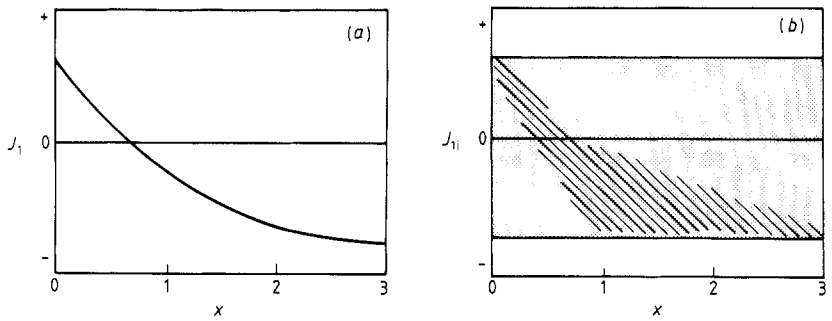

Figure 12. (*a*) Schematic representation of the dependence of the macroscopic intra-chain exchange constant J_1 on composition x as measured by static susceptibility methods (Visser 1988a). Samples with $x = 0$, 1, 1.5, 2.0 and 3.0 were used. (*b*) Schematic illustration of the distribution of individual Fe–Fe intra-chain exchange interactions, J_{1i}, as the composition x of $RbFeCl_{3-x}Br_x$ is varied. We have arbitrarily defined the upper and lower limits of J_{1i} as the bulk values, J_1, of the pure materials as discussed in the text. The more heavily shaded area denotes the most probably value of J_{1i} at a particular composition and this is based on the knowledge that the macroscopic exchange constant J_1 shown in figure 12(*a*) arises from the average of J_{1i} at a particular composition.

too that we have arbitrarily defined the upper and lower limits of J_{1i} as the values found in the pure compounds. It is possible that at intermediate compositions these boundaries are quite different. For instance, we do not expect a Fe–Cl_3–Fe bridge in an $x = 1.5$ sample necessarily to have the same value of J_{1i} as in an $x = 0$ sample.

(ii) There is a distinct remanence in the magnetisation measured parallel to the crystal c axis for $x = 2.0$ after the applied magnetic field had been raised to 5.6 T then returned to zero at a constant temperature of 2.0 K. This effect was much weaker for the $x = 1.5$ sample and could not be detected for the $x = 1.0$ sample. This indicates that at low temperature the $x = 2.0$ and to a lesser extent the $x = 1.5$ sample possess frozen magnetic disorder (Grest and Soukoulis 1983).

4.4. The magnetic phase diagram of $RbFeCl_{3-x}Br_x$

The interpretation of the neutron scattering and magnetisation measurements taken together is presented in the schematic magnetic phase diagram of figure 13. At intermediate compositions the exchange field is disrupted to such an extent that the system appears to have true singlet ground-state character. On the $RbFeBr_3$ side of the magnetic phase diagram the addition of approximately 10% of $RbFeCl_3$ ($x = 2.7$) destroys the magnetic long-range order and at 33% of $RbFeCl_3$ ($x = 2.0$) one observes a phase in which there is no detectable magnetic long-range order but in which there is remanent magnetic behaviour at 2.0 K. We shall tentatively call this a 'spin glass'. We have no estimate of the boundaries, either in temperature or composition, of this 'phase' other than a knowledge that it does not appear to exist for $RbFeCl_2Br$ ($x = 1.0$) at 2.0 K and that it does appear to exist for $RbFeClBr_2$ ($x = 2.0$) at the same temperature. Furthermore, we have no measure of the spatial magnetic homogeneity of this 'phase'. It is possible that $RbFeClBr_2$ at low temperatures is composed of regions behaving as singlet ground-state material and regions in which the induced moments are sufficiently large to support spin-glass 'ordering'.

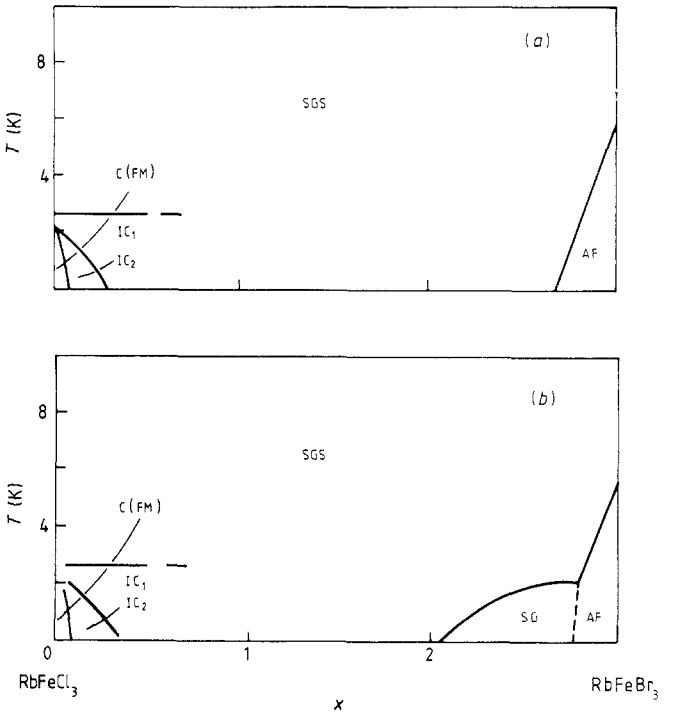

Figure 13. Schematic magnetic phase diagram for $RbFeCl_{3-x}Br_x$ showing two possibilities for the magnetic structure at intermediate compositions. (*a*) Only singlet ground-state (SGS) behaviour at intermediate composition is shown. (*b*) The case where there is a spin glass (SG) phase on the bromide side of the phase diagram. The remainder of the symbols have been explained in figure 11.

On the $RbFeCl_3$ side of the magnetic phase diagram there is the additional complication of IC phase formation. Boundaries between IC_1, IC_2 and C magnetic phases were deduced from a study of the satellite structures and this portion of the phase diagram is shown enlarged in figure 11. It must be stressed that these 'phases' contain magnetic correlations that are certainly spatially finite for the $x = 0.06$ and $x = 0.15$ samples and which may or may not be finite for the $x = 0.03$ sample.

The magnetic phase diagram of $RbFeCl_{3-x}Br_x$ may be extended and elucidated by the application of an external magnetic field parallel to the crystal c axis ($H \parallel c$). In the mixed singlet ground-state system $Rb_{1-x}Cs_xFeCl_3$ the application of $H \parallel c$ was found greatly to increase the magnetic correlation length (Harrison *et al* 1986a). By mixing the excited doublet into the ground singlet $H \parallel c$ compensates for the reduction of moments on iron atoms in the vicinity of Cs^+ impurities. Similarly, the application of a magnetic field parallel to the c axis of $RbFeCl_3$ should counteract the disruptive effect of either dopant with regard to the size of the induced moments; the combination of magnetic frustration and larger induced moments might then produce a spin glass at intermediate compositions. The character of such a glassy phase could be tuned by altering the magnitude of this applied magnetic field. We shall report a neutron scattering study of such effects in a forthcoming paper.

5. Conclusions

The mixed ferromagnet–antiferromagnet linear-chain compound $RbFeCl_3Br_x$ shows a complex array of magnetic ordering processes that depend on the composition x and temperature T. These phenomena may be rationalised qualitatively by considering the distribution of D/J_Q and γ/J_2 as a function of x.

The value of D/J_Q for the induced-moment magnets $RbFeCl_3$ and $RbFeBr_3$ is very close to the value at which a crossover from magnetic to singlet ground-state properties is expected. This sensitises the magnetic ordering processes to any impurities that disrupt the local magnetic exchange field J_Q. Magnetic correlations in the $x = 0.03$ sample at low temperatures were found to be finite, in contrast to the predictions of molecular-field-based models such as that of Hone *et al* (1975). Consequently, the magnetic phase diagrams are different from those predicted by Fishman and Aharony (1979) for a mixed ferromagnet–antiferromagnet. At intermediate compositions one observes a singlet ground-state phase rather than a spin-glass phase. It is possible that when a magnetic field is applied parallel to the crystal c axis of these materials there will be the necessary combination of quenched spatial disorder and magnetic frustration necessary for spin-glass formation to occur.

Acknowledgments

We thank the UK Science and Engineering Research Council for financial support. AH is grateful to St John's College, Oxford, for further financial support. We also wish to thank Professor K R A Ziebeck of ILL (now at Loughborough University of Technology) for assistance with the neutron scattering experiments and Dr P Day (Oxford) for encouragement throughout the project and for interesting discussions. Our thanks are also due to Dr T E Wood for bringing our attention to this system initially.

References

Adachi K, Takeda K, Matsubara F, Mekata M and Haseda T 1983 *J. Phys. Soc. Japan* **52** 2202
Aeppli G, Shapiro S M, Birgeneau R J and Chen H S 1982 *Phys. Rev.* B **25** 4882
Baines J A, Johnson C A and Thomas M F 1983 *J. Phys. C: Solid State Phys.* **16** 3579
Bevaart L, Frikee E, Lebesque J V and de Jongh L J 1978 *Phys. Rev.* B **18** 3376
Bevaart L, Tegelaar P M L H, van Duyneveldt A J and Steiner M 1983 *J. Magn. Magn. Mater.* **31–34** 1447
Birgeneau R J, Cowley R A, Shirane G and Yoshizawa H 1984 *J. Stat. Phys.* **34** 817
Bloch D 1966 *J. Phys. Chem. Solids* **27** 881
Boersma F, de Jonge W J M and Kopinga K 1981 *Phys. Rev.* B **23** 186
Bontemps N, Grisolia C, Nerozzi M and Briat B 1982 *J. Appl. Phys.* **53** 2710
Brand R A, Georges-Gibert H, Hubsch J and Heller J A 1985 *J. Phys. F: Met. Phys.* **15** 1987
Cheetham A K and Skarnulis A J 1981 *Anal. Chem.* **53** 1060
Chen J H and Lubensky T C 1977 *Phys. Rev.* B **16** 2106
Defotis G C and Mantis D S 1986 *J. Magn. Magn. Mater.* **54–57** 79
Eibschutz M, Davidson G R and Cox D E 1973 *AIP Conf. Proc.* **18** 386
Eibschutz M, Lines M E and Sherwood R C 1975 *Phys. Rev.* B **11** 4595
Fishman S and Aharony A 1979 *Phys. Rev.* B **19** 3776
Grest G S and Soukoulis C M 1983 *Springer Series in Solid State Sciences* vol 48, ed. M Ausloos and R J Elliott (Berlin: Springer) p 223

Harrison A 1987 *J. Phys. C: Solid State Phys.* **20** 6287
Harrison A and Visser D 1988a *J. Phys. C: Solid State Phys.* submitted
—— 1988b *J. Phys. C: Solid State Phys.* submitted
Harrison A, Visser D, Day P, Knop W and Steiner M 1986a *J. Phys. C: Solid State Phys.* **19** 6811
Harrison A, Visser D, Day P and Ziebeck K R A 1986b *J. Magn. Magn. Mater.* **54–57** 1273
Hayase S, Futamara R, Sakashita H and Terauchi H 1985 *J. Phys. Soc. Japan* **54** 812
Hirakawa K, Kadowaki H and Ubukoshi K 1983 *J. Phys. Soc. Japan* **52** 1814
Hone D, Montano P A, Tonegawa T and Imry Y 1975 *Phys. Rev.* B **12** 5141
Hubsch J and Gavoille G 1982 *Phys. Rev.* B **26** 3815
Hubsch J, Gavoille G and Bolfa J 1978 *J. Appl. Phys.* **49** 1363
Katsumata K 1986 *J. Magn. Magn. Mater.* **54–57** 75
Katsumata K, Nire T, Tanimoto M and Yoshizawa H 1982 *Phys. Rev.* B **25** 428
Kettler P, Steiner M, Dachs H, Germer R and Wanklyn B 1981 *Phys. Rev. Lett.* **47** 1329
Kimishima Y, Ikeda H, Furukawa A and Nagoro H 1986 *J. Phys. Soc. Japan* **55** 3574
Knop W, Steiner M and Day P 1983 *J. Magn. Magn. Mater.* **31–34** 1033
Loidl A, Mullner M, McIntyre G J, Knorr K and Jex H 1985 *Solid State Commun.* **54** 367
Lines M E 1974 *Phys. Rev.* B **9** 3827
Lines M E and Eibschutz M 1975 *Phys. Rev.* B **11** 4583
Maletta H 1982 *J. Appl. Phys.* **53** 2185
Maletta H, Aeppli G and Shapiro S M 1982 *Phys. Rev. Lett.* **48** 1490
Maletta H and Felsch W 1980 *Z. Phys.* B **37** 55
Matsubara F 1985 *J. Phys. Soc. Japan* **54** 1677
Medvedev M V and Rumyantsev E L 1978 *Phys. Status Solidi* b **85** 427
Mekata M, Ajiro Y and Adachi K 1986 *J. Magn. Magn. Mater.* **54–57** 1265
Munninghof G, Hellner E, Treutmann W, Lehner N and Heger G 1984 *J. Phys. C: Solid State Phys.* **17** 1281
Pappa C, Hammann J and Jacoboni C 1984 *J. Phys. C: Solid State Phys.* **17** 1303
Rhyne J J, Pickart S J and Alperin H A 1972 *Phys. Rev. Lett.* **29** 1562
Sellmyer D J and Nafis S 1986 *J. Magn. Magn. Mater.* **54–57** 113
Sherrington D 1983 *Springer Lecture Notes in Physics* vol 192, ed. J L van Hemmen and I Morgenstern (Berlin: Springer) p 348
Shiba H 1982 *Solid State Commun.* **41** 511
Shiba H and Suzuki N 1983 *J. Phys. Soc. Japan* **52** 1383
Steiner M and Axmann A 1976 *Solid State Commun.* **19** 115
Suzuki N 1983 *J. Phys. Soc. Japan* **52** 3907
Takeda K and Schouten J C 1981 *J. Phys. Soc. Japan* **50** 2554
Toulouse G 1977 *Commun. Phys.* **2** 115
Villain J 1979 *Z. Phys.* B **33** 31
Visser D 1988a *J. Phys. C: Solid State Phys.* submitted
Visser D 1988b unpublished work
Visser D, Brown P J and Ziebeck K R A 1985 *Annex to the ILL Annual Report* p 93
Visser D and Harrison A 1982 unpublished results
Visser D, Harrison A and McIntyre G J 1988 *Proc. Int. Conf. Magnetism: J. Physique Coll.* at press
Visser D and Knop W 1988 unpublished observations
Visser D and McIntyre G J 1988 *Proc. Int. Conf. Neutron Scattering (Paris) 1988*
Visser D and Prodan A 1980 *Phys. Status Solidi* a **58** 481
Visser D, Verschoor G C and IJdo D W J 1980 *Acta Crystallogr.* B **36** 28
Wada M, Ubukoshi K and Hirakawa K 1982 *J. Phys. Soc. Japan* **51** 283
Wiedenmann A, Burlet P, Scheuer H and Convert P 1981 *Solid State Commun.* **38** 129
Wiedenmann A, Gunsser W, Burlet P and Mezei F 1983 *J. Magn. Magn. Mater.* **31–34** 1395
Wong P Z, Horn P M, Birgeneau R J, Safinya C R and Shirane G 1980 *Phys. Rev. Lett.* **45** 1974
Wong P Z, von Molnar S, Palstra T T M, Mydosh J A, Yoshizawa H, Shapiro S M and Ito A 1985 *Phys. Rev. Lett.* **55** 2043